Journal of Solid State Chemistry **164,** 42–50 (2002)
doi:10.1006/jssc.2001.9446, available online at http://www.idealibrary.com on IDEAL®

Hydrothermal Synthesis, Single-Crystal Structure Analysis, and Solid-State NMR Characterization of $Zn_2(OH)_{0.14(3)}F_{0.86(3)}(PO_4)$

Karen Inge Taasti,* Axel Nørlund Christensen,*,[1] Poul Norby,† Jonathan C. Hanson,‡ Bente Lebech,§ Hans J. Jakobsen,¶ and Jørgen Skibsted¶

*Department of Inorganic Chemistry, University of Aarhus, DK-8000 Aarhus C, Denmark; †Department of Chemistry, University of Oslo, Blindern, N-0315 Oslo, Norway; ‡Department of Chemistry, Brookhaven National Laboratory, Upton, New York 11973-5000i; §Condensed Matter Chemistry and Physics Department, Risø National Laboratory, DK-4000 Roskilde, Denmark; and ¶Instrument Centre for Solid-State NMR Spectroscopy, Department of Chemistry, University of Aarhus, DK-8000 Aarhus C, Denmark

Received July 2, 2001; in revised form October 25, 2001; accepted November 1, 2001

The zinc fluoro phosphate $Zn_2F(PO_4)$ has been produced by hydrothermal synthesis employing hydrofluoric acid as a mineralizer in a H_2O or D_2O medium. A single-crystal X-ray synchrotron diffraction analysis of $Zn_2F(PO_4)$ shows that the zinc fluoro phosphate is monoclinic, $a = 9.690(1)$, $b = 12.793(1)$, and $c = 11.972(1)$ Å, $\beta = 108.265(1)^\circ$, space group $P2_1/c$, No. 14, $Z = 16$. Reflections hkl with $k = 2n + 1$ are weak but significant and the structure shows pseudosymmetry. $Zn_2F(PO_4)$ has the wagnerite-type $M_2F(XO_4)$ structure with four Zn atoms each coordinated to four O atoms and one F atom while four other Zn atoms are coordinated to four O atoms and two F atoms. A difference Fourier map, calculated from the single-crystal X-ray data, shows additional electron density close to the four fluorine atoms, indicating a possible partial substitution of F^- by OH^- ions. This is unambiguously confirmed by $^{31}P-\{^1H\}$ cross-polarization magic-angle spinning (MAS) and by $^1H/^2H$ MAS NMR spectroscopy. The narrow line width observed for the ^1H resonance and the unique set of ^2H quadrupole coupling parameters (obtained for the $Zn_2F(PO_4)$ sample using D_2O as medium) show that $^1H/^2H$ is present as OH(D) groups rather than as water of crystallization in the structure. Quantitative ^1H MAS NMR analysis shows that the composition of the sample is $Zn_2(OH)_{0.14(3)}F_{0.86(3)}(PO_4)$. The high-speed ^{19}F MAS NMR spectrum exhibits two resolved resonances with equal intensity, which are ascribed to an overlap of resonances from the four distinct fluorine sites in $Zn_2(OH)_{0.14(3)}F_{0.86(3)}(PO_4)$.

INTRODUCTION

Microporous compounds with open framework structures such as zeolites and aluminophosphates are often made by hydrothermal or organothermal synthesis and are in several cases obtained only as powders. For this type of syntheses, the application of organic additives as structure-directing agents (1, 2) and the use of hydrofluoric acid as a mineralizer (3, 4) have resulted in the synthesis of several new compounds, especially zeolites, aluminophosphates, and metal-ion-substituted aluminophosphates. In many cases the use of hydrofluoric acid as a mineralizer results in crystals sufficiently large for structure determination by single-crystal X-ray diffraction. In this work we have employed this approach to synthesize the zinc fluoro phosphate, $Zn_2F(PO_4)$, and report the preparation, crystal structure, and a multinuclear (^1H, ^2H, ^{19}F, ^{31}P) solid-state NMR study of this new phase. Furthermore, we found that $Zn_2F(PO_4)$ is formed as a pure phase in attempts to substitute Zn^{2+} ions for Al^{3+} ions in microporous $AlPO_4$ materials such as $AlPO_4$-35, using hydrofluoric acid as a mineralizer.

Solid-state NMR techniques, particularly those involving magic-angle spinning and $X-\{^1H\}$ cross-polarization (CP), have provided considerable insight into the structure of several important inorganic materials such as gels, ceramics, catalysts, microporous materials, and minerals (5). Furthermore, the combination of solid-state NMR and X-ray diffraction techniques may often give a more detailed description of the structure and composition of microcrystalline materials, since NMR spectroscopy is most sensitive to the local ordering of the structure. In the present work solid-state NMR is found to be particularly useful in the detection and quantification of the low degree of OH^- for F^- substitution in the structure of $Zn_2F(PO_4)$.

$Zn_2F(PO_4)$ belongs to the group of metal phosphates with the general formula $M_2X(PO_4)$ where the anion X^- can be OH^- or F^- and M typically is a divalent metal ion. Several of these phosphates occur as minerals such as tarbuttite ($Zn_2(OH)PO_4$) (6), libethenite ($Cu_2(OH)PO_4$) (7), wagnerite (Mg_2FPO_4) (8), and herderite ($CaBeFPO_4$) (9).

[1]To whom correspondence should be addressed. E-mail: anc@chem.au.dk.

0022-4596/02 $35.00

Several others have been made synthetically including Mn_2FPO_4 (10, 11), Cd_2FPO_4 (12), Cu_2FPO_4 (13), and β-$Mg_2(OH)PO_4$ (14). Most recently, $Co_2(OH)PO_4$ (15), $Zn_2(OH)PO_4$ (15), and Co_2FPO_4 (11) have been prepared by hydrothermal synthesis employing organic additives as structure-directing agents. The structural chemistry of the $M_2X(PO_4)$ phosphates is rather complex, however: the structures generally contain a condensed network of vertex- and edge-sharing MO_5, MO_6, and PO_4 subunits. A main class of phosphates are those isomorphous with adamite ($Zn_2(OH)AsO_4$, orthorhombic, *Pnnm* (16)) which include $Zn_2(OH)PO_4$, $Cu_2(OH)PO_4$, and $Co_2(OH)PO_4$ (6, 7, 15) while another group includes those isomorphous with wagnerite (Mg_2FPO_4, monoclinic, $P2_1/c$ (8)), i.e., Co_2FPO_4 and β-$Mg_2(OH)PO_4$ (13, 14). The above-mentioned structures are thus formed for metal fluoro phosphates as well as for metal hydroxy phosphates. In this work we show that $Zn_2F(PO_4)$ belongs to the wagnerite-type of phosphates with a small degree of substitution of OH^- for F^- ions for the samples investigated.

EXPERIMENTAL

The zinc fluoro phosphate $Zn_2F(PO_4)$ was prepared by hydrothermal synthesis using $Zn(CH_3COO)_2 \cdot 2H_2O$, 85% H_3PO_4, and HF from Merck and 1,4-diazabicyclo-[2.2.2]octane (DABCO) from Aldrich. Two samples were prepared employing either demineralized water or D_2O (99.7% from Hydro) as solvent. The synthesis employed the following molar ratio for the reagents: 1.0 $Zn(CH_3COO)_2 \cdot 2H_2O$:2.0 H_3PO_4:1.90 HF:1.6 DABCO: 300 H_2O/D_2O. After mixing of the reagents pH values of 4.7 and 4.8 were measured for the mixtures containing H_2O and D_2O, respectively. The mixtures were heated in Teflon-lined pressure vessels using a reaction temperature of 180°C for 103 h. The products were washed with H_2O and D_2O and dried in air at room temperature.

X-ray powder patterns at 25°C were obtained on a Stoe-Stadi diffractometer using Cu$K\alpha_1$ radiation ($\lambda = 1.5406$ Å). A transmission mode was applied with a flat sample on tape. The diffractometer was calibrated with an external silicon standard ($a_{Si} = 5.43050$ Å). The counter was a curved position-sensitive detector covering 40° in 2θ or a linear detector covering 5° in 2θ and used in a step scan mode. Single-crystal X-ray diffraction data for $Zn_2F(PO_4)$ prepared in the H_2O medium were obtained at the beam line X7B at the National Synchrotron Light Source, Brookhaven National Laboratory, using a MAR detector.

The infrared spectrum was obtained on a Perkin Elmer Paragon 1000 FT-IR spectrometer. The spectrum indicated that the sample contains OH^- groups. ^1H, ^2H, and ^{31}P MAS and the ^{31}P–$\{^1H\}$ CP/MAS NMR spectra were recorded on a Varian INOVA-400 (9.4 T) spectrometer using home-built CP/MAS NMR probes for 4- and 5-mm o.d. rotors while the ^{19}F MAS spectrum was obtained on a Varian INOVA-300 (7.1 T) spectrometer using a home-built CP/MAS NMR probe for 5-mm-o.d. rotors and with transmission-line tuning for the high-frequency channel. This channel employed an rf field strength of $\gamma B_1/2\pi = 100$ kHz for the ^{19}F MAS spectra. The ^1H and ^{31}P MAS NMR experiments employed 45° excitation pulses for rf field strengths of $\gamma B_1/2\pi = 70$ kHz and $\gamma B_1/2\pi = 50$ kHz, respectively, while the ^2H MAS NMR spectrum was obtained with a short (1.0 μs) excitation pulse for $\gamma B_1/2\pi = 50$ kHz. The ^{31}P–$\{^1H\}$ CP/MAS NMR spectrum employed $\gamma B_2/2\pi = 55$ kHz during ^1H decoupling and $\gamma B_2/2\pi = \gamma B_1/2\pi = 40$ kHz for the Hartmann–Hahn match, a CP contact time of 0.5 ms, and a 30-s relaxation delay. The quantitative analysis for the ^1H MAS NMR experiments, obtained with the spinning speed $\nu_R = 15.0$ kHz, employed $CH_3COONa \cdot 3H_2O$ and Na_2HPO_4 as external reference samples for normalization of the intensities. ^1H, ^{19}F, and ^{31}P isotropic chemical shifts (ppm) are relative to external samples of neat tetramethyl silane (TMS), neat $CFCl_3$, and 85% H_3PO_4, respectively. Simulations and least-squares optimizations of the ^2H MAS NMR spectrum were performed using software described elsewhere (17, 18).

RESULTS AND DISCUSSION

Synthesis

To improve the catalytical properties of microporous $AlPO_4$ materials, there is an ongoing interest in substituting some of the aluminum atoms with divalent metal ions such as Mg^{2+}, Co^{2+}, and Zn^{2+}. Such substitution results in an increased acidity of the compounds since the excess negative charge of the framework is compensated for by protons. For $AlPO_4$-35, which has the same structure as the zeolite levyne (19), it has been shown that a silicon-substituted analogue (SAPO-35) can be synthesized using the amine 1,4-diazabicyclo[2.2.2]octane as template (20). In this work we have used the same template in hydrothermal synthesis of a Zn-substituted form of $AlPO_4$-35, i.e., ZnAPO-35. However, the hydrothermal synthesis of ZnAPO-35 did not result in products with single crystals large enough for traditional single-crystal X-ray diffraction analysis and the use of hydrofluoric acid as a mineralizer had only a marginal effect on the size of the crystals in the reaction products. X-ray fluorescence analysis indicated a degree of Zn substitution corresponding to the ratio Zn:Al = 0.28:0.72. An attempt to produce a Zn analogue of $AlPO_4$-35, where all Al^{3+} are replaced by Zn^{2+} ions, resulted in the formation of a pure crystalline compound. From the powder XRD pattern, this phase was found to be the zinc fluoro phosphate $Zn_2F(PO_4)$ using the ICDD database (card no. 24-1442). The use of hydrofluoric acid as mineralizer in this synthesis gave large crystals of $Zn_2F(PO_4)$ and a crystal

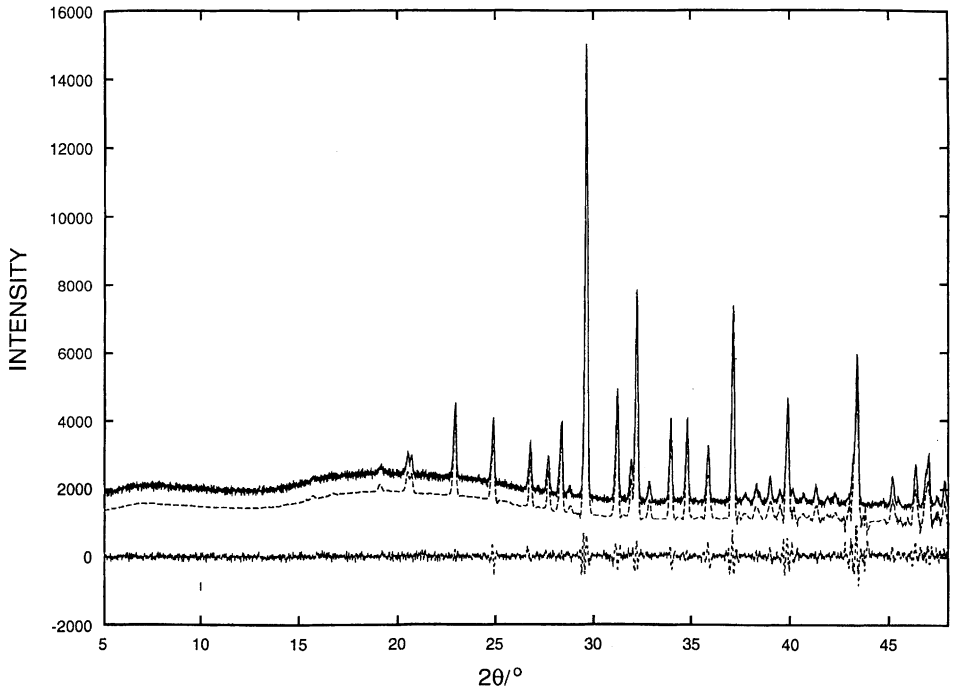

FIG. 1. X-ray diffraction powder pattern of $Zn_2(OH)_{0.14(3)}F_{0.86(3)}(PO_4)$. The upper and lower curves represent the observed and calculated profiles, respectively, with the difference in the lower part of the figure. The range in 2θ is 5–48°. $\lambda = 1.5406$ Å.

with the size $0.08 \times 0.04 \times 0.04\ mm^3$ was picked from the reaction product for single-crystal X-ray analysis.

X-Ray Diffraction

The X-ray diffraction powder pattern of $Zn_2F(PO_4)$, shown in Fig. 1 (and listed in Table 1), is indexed in the monoclinic space group $P2_1/c$ using the unit cell data from the single-crystal analysis given in Table 2. The XRD pattern from the profile refinement and the corresponding difference plot (Fig. 1) are calculated using the program ALLHKL (21). The result of the indexing of the pattern, using the program DICVOL (22), is listed in Table 1 and shows that reflections are observed only for $k = 2n$. The first low-angle reflections observed in the X-ray powder pattern are the reflections 021 at $2\theta = 15.89°$ and 200 at $2\theta = 19.30°$. These two reflections are weak. The 020 reflection at $2\theta = 13.84°$ is not observed. This indicates a pseudosymmetry of the structure, where the packing of all atoms in the unit cell from $b = 0$ to $b = 0.5$ is similar to the packing of the atoms in the cell from $b = 0.5$ to $b = 1.0$.

The single-crystal X-ray data, obtained for a crystal produced in a H_2O medium, were used to solve the structure by direct methods using the SIR program (23), which gives the positions of all atoms. The unit cell data and relevant crystallographic parameters are summarized in Tables 2 and 3. A difference Fourier map shows some additional electron density close to the four fluorine atoms, which may originate from partial substitution of F^- by OH^- ions. However, the additional four-electron density peaks in the difference Fourier map are in all cases higher than those corresponding to electrons from a hydrogen atom. Thus,

TABLE 1
X-Ray Powder Data for $Zn_2F(PO_4)$[a]

$2\theta_{obs}$	$2\theta_{calc}$	d_{obs}	d_{calc}	I_{obs}	h	k	l
15.89	15.87	5.573	5.581	1	0	2	1
19.30	19.30	4.595	4.596	2	2	0	0
20.69	20.69	4.290	4.291	3	2	0	−2
20.89	20.85	4.249	4.258	2	1	2	−2
23.07	23.08	3.852	3.850	16	2	2	−1
25.02	25.02	3.556	3.556	14	1	2	2
26.93	26.93	3.308	3.308	10	2	2	1
27.32	27.34	3.262	3.260	2	0	2	3
27.85	27.83	3.201	3.203	8	0	4	0
28.51	28.51	3.128	3.128	16	2	0	2
28.95	28.96	3.082	3.081	2	2	2	−3
29.76	29.75	3.000	3.001	100	1	4	−1
31.34	31.37	2.852	2.850	24	2	0	−4
32.07	32.05	2.789	2.791	8	0	4	2
32.34	32.34	2.766	2.766	46	3	2	0
33.05	33.02	2.708	2.711	4	1	2	−4
34.09	34.09	2.628	2.628	17	2	4	0
34.92	34.93	2.567	2.567	17	2	4	−2
36.00	36.00	2.493	2.493	12	1	4	−3
37.24	37.30	2.413	2.409	42	4	0	−2
37.87	37.84	2.374	2.376	2	2	2	3
38.44	38.45	2.340	2.339	3	3	2	−4

[a] Monoclinic unit cell $a = 9.690(3)$, $b = 12.804(5)$, and $c = 11.97(1)$ Å, $\beta = 108.27(6)°$, figure of merit $M(22) = 8.7$.

TABLE 2
Experimental Data and Unit Cell Parameters for the Single-Crystal Measurements on $Zn_2F(PO_4)$

a/Å	9.690(1)
b/Å	12.793(1)
c/Å	11.972(1)
β/°	108.265(1)
Cell volume/Å^3	1409
Space group	$P2_1/c$
Z	16
λ/Å	0.9355
Density (calc)/g cm^{-3}	4.62
Size of crystal/mm	$0.08 \times 0.04 \times 0.04$
Linear absorption coeff. μ/cm^{-1}	117
No. of independent reflections with $I > 3\sigma(I)$	1153
$R(F)$/%	5.7
T/°C	25

a model has been examined where the fluorine atoms each are placed statistically in two sites, F1 and F11, F2 and F21, F3 and F31, F4 and F41, employing the program LINUS (24) with scattering contributions from neutral atoms. The occupancies for these eight atoms have been refined with the thermal displacement parameters of the atoms fixed. The refinement shows that the four sets of positions for fluorine atoms represent one atom for each of the four sets of coordinates. The result of the analysis is given by the refined atomic coordinates and anisotropic temperature factors for $Zn_2F(PO_4)$ in Table 3 and by the selected bond distances in Table 4. Figure 2 illustrates how the eight Zn and four P atoms are linked together. Only the Zn and P atoms are labeled in this drawing. The atoms P1, P2, P3, and P4 have the coordinates listed in Table 3. The positions of the a–c axes of the unit cell are indicated. There is an approximate

TABLE 3
Refined Positional and Thermal Displacement Parameters for the Structure of $Zn_4F(PO_4)$

Atom	Occupancy	x/a	y/b	z/c	u_{11}[a]	u_{22}	u_{33}	u_{12}	u_{13}	u_{23}
Zn1		0.5419(2)	0.0723(2)	0.4064(1)	0.016(1)	0.005(1)	0.020(1)	0.002(1)	0.007(1)	0.000(1)
Zn2		0.4488(2)	0.0742(2)	0.0856(1)	0.012(1)	0.005(1)	0.018(1)	−0.001(1)	0.005(1)	0.000(1)
Zn3		0.0424(2)	0.1767(2)	0.4004(1)	0.016(1)	0.006(1)	0.012(1)	0.000(1)	0.004(1)	0.002(1)
Zn4		0.9542(2)	0.1796(2)	0.0823(1)	0.016(1)	0.005(1)	0.015(1)	−0.001(1)	0.004(1)	0.000(1)
Zn5		0.2050(2)	0.0073(2)	0.6911(1)	0.014(1)	0.013(1)	0.013(1)	−0.002(1)	0.004(1)	−0.005(1)
Zn6		0.8063(2)	0.0164(1)	0.8104(1)	0.013(1)	0.011(1)	0.012(1)	0.001(1)	0.002(1)	0.002(1)
Zn7		0.2983(2)	0.2425(1)	0.8060(1)	0.014(1)	0.013(1)	0.010(1)	−0.001(1)	0.004(1)	−0.003(1)
Zn8		0.6970(2)	0.2342(1)	0.6891(1)	0.012(1)	0.011(1)	0.011(1)	0.002(1)	0.005(1)	0.003(1)
P1		0.1207(5)	0.0725(3)	0.9251(2)	0.0071(7)					
P2		0.8826(5)	0.0751(3)	0.5733(3)	0.0070(7)					
P3		0.3831(5)	0.1753(3)	0.5781(2)	0.0046(7)					
P4		0.6171(5)	0.1734(3)	0.9223(2)	0.0045(7)					
O11		0.194(1)	0.0968(6)	0.8295(7)	0.013(2)					
O12		0.235(1)	0.0497(8)	1.0419(8)	0.015(2)					
O13		0.024(1)	0.1656(7)	0.9367(7)	0.017(2)					
O14		0.016(1)	−0.0198(7)	0.8836(8)	0.013(2)					
O21		0.760(1)	0.0440(8)	0.4650(8)	0.013(2)					
O22		0.822(1)	0.1085(6)	0.6747(7)	0.012(2)					
O23		0.975(1)	0.1667(7)	0.5497(7)	0.014(2)					
O24		0.988(1)	−0.0153(7)	0.6204(8)	0.009(2)					
O31		0.267(1)	0.1994(7)	0.4591(7)	0.006(2)					
O32		0.308(1)	0.1503(7)	0.6660(7)	0.011(2)					
O33		0.482(1)	0.2723(8)	0.6212(8)	0.013(2)					
O34		0.480(1)	0.0890(7)	0.5600(7)	0.009(2)					
O41		0.689(1)	0.1435(6)	0.8330(7)	0.010(2)					
O42		0.735(1)	0.1970(7)	1.0406(7)	0.005(2)					
O43		0.521(1)	0.2702(8)	0.8798(8)	0.013(2)					
O44		0.524(1)	0.0864(7)	0.9450(7)	0.011(2)					
F1	0.87(2)	0.086(1)	0.2063(6)	0.2409(6)	0.012					
F2	0.68(3)	0.584(1)	0.0460(8)	0.2447(8)	0.012					
F3	0.83(2)	0.827(1)	0.1616(6)	0.2834(6)	0.012					
F4	0.74(2)	0.330(2)	0.0859(8)	0.2854(8)	0.012					
F11	0.12(2)	0.175(7)	0.158(4)	0.209(4)	0.012					
F21	0.26(1)	0.625(5)	0.071(3)	0.226(3)	0.012					
F31	0.18(2)	0.914(5)	0.213(3)	0.258(3)	0.012					
F41	0.23(4)	0.369(7)	0.070(4)	0.271(4)	0.012					

[a]Isotropic thermal displacement parameters for all nonmetal atoms.

TABLE 4
Selected Bond Distances (Å) for $Zn_2(PO_4)$

Zn1–O21	2.04(1)	
Zn1–O43^i	2.04(1)	$i = x, \frac{1}{2} - y, -\frac{1}{2} + z$
Zn1–O34	2.11(1)	
Zn1–F4	2.12(1)	
Zn1–F2	2.13(1)	
Zn1–O34^i	2.13(1)	$i = 1 - x, -y, 1 - z$
Zn3–O23^i	2.07(1)	$i = -1 + x, y, z$
Zn3–O31	2.08(1)	
Zn3–O13^i	2.08(1)	$i = x, \frac{1}{2} - y, -\frac{1}{2} + z$
Zn3–O24^i	2.09(1)	$i = 1 - x, -y, 1 - z$
Zn3–F1	2.12(1)	
Zn3–F3^i	2.13(1)	$i = -1 + x, y, z$
Zn5–O24^i	2.02(1)	$i = -1 + x$, y, z
Zn5–O11	2.05(1)	
Zn5–F2^i	2.06(1)	$i = 1 - x, -y, 1 - z$
Zn5–O21^i	2.11(1)	$i = 1 - x, -y, 1 - z$
Zn5–O32	2.15(1)	
Zn5–F3^i	2.22(1)	$i = 1 - x, -y, 1 - z$
Zn7–F1^i	2.06(1)	$i = x, \frac{1}{2} - y, \frac{1}{2} + z$
Zn7–O32	2.08(1)	
Zn7–O31^i	2.09(1)	$i = x, \frac{1}{2} - y, \frac{1}{2} + z$
Zn7–O43	2.09(1)	
Zn7–O11	2.18(1)	
Zn7–F4^i	2.24(1)	$i = x, \frac{1}{2} - y, \frac{1}{2} + z$
Zn2–F2	1.98(1)	
Zn2–O12^i	1.99(1)	$i = x, y, -1 + z$
Zn2–O33^i	2.01(1)	$i = x, \frac{1}{2} - y, -\frac{1}{2} + z$
Zn2–O44^i	2.04(1)	$i = x, y, -1 + z$
Zn2–O44^i	2.12(1)	$i = 1 - x, -y, 1 - z$
Zn4–F1^i	1.96(1)	$i = 1 + x, y, z$
Zn4–O23^i	2.03(1)	$i = x, \frac{1}{2} - y, -\frac{1}{2} + z$
Zn4–O42^i	2.03(1)	$i = x, y, -1 + z$
Zn4–O13^i	2.06(1)	$i = 1 + x, y, -1 + z$
Zn4–O14^i	2.09(1)	$i = 1 - x, -y, 1 - z$
Zn6–F4^i	1.96(1)	$i = 1 - x, -y, 1 - z$
Zn6–O14^i	2.00(1)	$i = 1 + x, y, z$
Zn6–O22	2.05(1)	
Zn6–O41	2.05(1)	
Zn6–O12^i	2.11(1)	$i = 1 - x, -y, 2 - z$
Zn8–F3^i	1.94(1)	$i = x, \frac{1}{2} - y, \frac{1}{2} + z$
Zn8–O33	2.05(1)	
Zn8–O22	2.05(1)	
Zn8–O41	2.10(1)	
Zn8–O42^i	2.12(1)	$i = x, \frac{1}{2} - y, -\frac{1}{2} + z$
P1–O12	1.52(1)	P2–O21 1.51(1)
P1–O14	1.53(1)	P2–O24 1.53(1)
P1–O13	1.55(1)	P2–O23 1.56(1)
P1–O11	1.55(1)	P2–O22 1.57(1)
P3–O32	1.49(1)	P4–O41 1.50(1)
P3–O34	1.51(1)	P4–O44 1.51(1)
P3–O31	1.55(1)	P4–O43 1.54(1)
P3–O33	1.55(1)	P4–O42 1.55(1)

2-fold axis coincidental with the 2_1 screw axis. There is a central $Zn_2(PO_4)_2$ corner-sharing ring Zn7–P4–Zn8–P3 with a similar $Zn_2(PO_4)_2$ corner-sharing ring on either side (Zn1–P3–Zn8–P2 and Zn2–P4–Zn7–P1). In addition, there is a pair of edge-sharing zinc polyhedra bridging the 4-rings (Zn5–Zn7) and (Zn8–Zn6). The 2-fold symmetry breaks down with a second edge-sharing zinc polyhedron on one side (Zn7–Zn3) which does not close on the other side (Zn8–Zn4). The broken bond is one of the disordered F1 atoms. Figure 3 is a projection of the structure along the [010] direction, tilted a few degrees from that direction. In the list of bond lengths (Table 4) and in this figure the set of fluorine atoms with the lowest occupancy has been omitted. The structure show pseudosymmetry and has a packing of atoms in the unit cell in the range of b from 0.0 to 0.5 rather similar to the packing for the range for b from 0.5 to 1.0. This can be illustrated with the set of coordinates for the atoms Zn1 and Zn2, where the Zn1 coordinates are 0.5419(2), 0.0723(2), 0.4064(1), and symmetry related Zn2 to the atom listed in Table 2 with the coordinates 0.5512(1), 0.57428(2), 0.4144(1) and similar for the remaining 15 sets of coordinates. For this reason a projection along the [010] direction is rather confused as the atoms are seen on top of each other. Figure 3 displays only half the content of the unit cell. The full content of the unit cell is displayed in the figure in the graphical abstract.

$Zn_2F(PO_4)$ has the wagnerite structure and is isostructural to $Mg_2F(PO_4)$ (8) and $Co_2F(PO_4)$ (11). The structure has four zinc atoms each coordinated to four oxygens and one F(OH) atom and four zinc atoms coordinated to four oxygens and two F(OH) atoms. The Zn–O distances are comparable to the Zn–O distances reported for zinc phosphates with framework structures (25, 26) where the distances are in the range from 1.88(1) to 1.99(1) Å. In $Zn_2(OH)(PO_4)$ with the adamite-type structure (15) the Zn–O distances are in the range 2.002(4) to 2.070(4) Å with a long Zn–O bond length of 2.296(3) Å from an axial distortion of a ZnO_6 octahedron. However, the interatomic distances in the zinc coordination polyhedra of $Zn_2F(PO_4)$ show a larger variation than in the structures referred to above (15, 25, 26) as a result of the limited set of data measured on the small crystal and the statistical disorder in the structure. Reflections were observed out to sin $\Theta/\lambda = 0.55$, but only 1153 reflections had $I > 3\sigma(I)$.

Neutron Diffraction

The neutron diffraction powder pattern (Fig. 4) has been used to test a possible OD^-/F^- substitution in the sample. Neutron diffraction powder patterns have been calculated using the program LAZY PULVERIX (27) for the following models: (i) a model using the atomic coordinates listed in Table 3, (ii) an ordered model where the atoms F1, F2, F3, F4 have the occupancies 1.0 and the atoms F11, F21, F31,

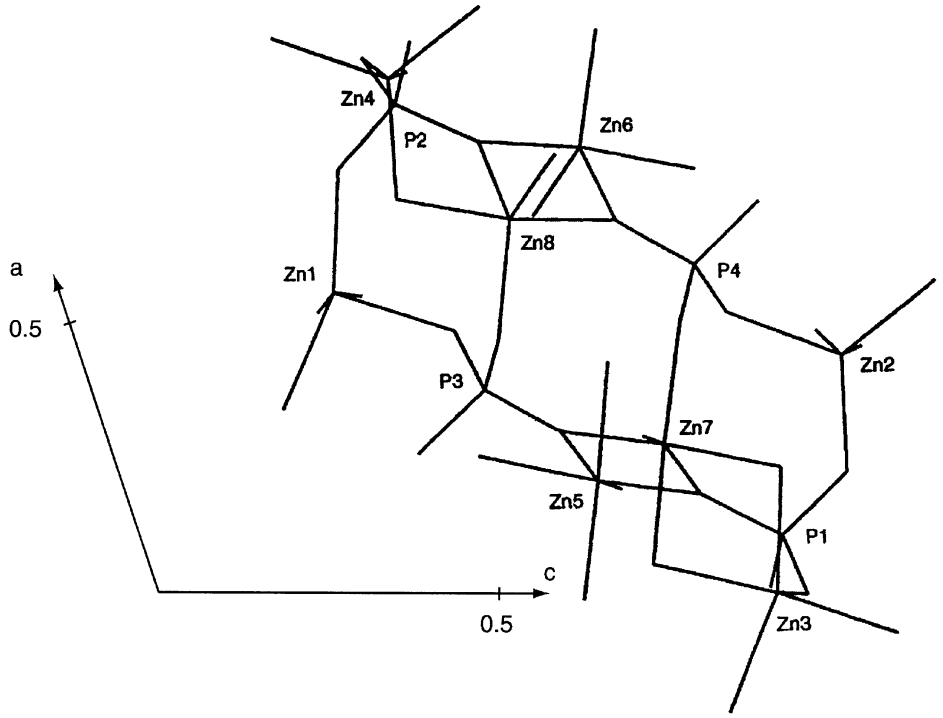

FIG. 2. Drawing showing how the eight Zn and four P polyhedra are linked together in the structure of $Zn_2F(PO_4)$. Only the Zn and P atoms are labeled in the drawing.

F41 were omitted, and (iii) a disordered model corresponding to the composition $Zn_2(OD)_{0.14(3)}F_{0.86(3)}(PO_4)$ (*vide infra*) where the deuterium atoms are placed at the positions of the atoms F11, F21, F31, F41 with the occupancy 0.14 and oxygen and fluorine atoms are placed with the occupancies 0.14 and 0.86, respectively, in the F1, F2, F3, F4 atom positions. The powder patterns calculated using these three models deviate only marginally from one another. Thus, a fourth pattern has been calculated for the composition $Zn_2OD(PO_4)$ with oxygen atoms in the F1, F2, F3, F4 positions, and deuterium atoms in the F11, F21, F31, F41 positions. This powder pattern differs significantly from the three other patterns. Profile refinements have been used in the model calculations with the program GSAS (28) and the positional parameters listed in Table 3. The scattering lengths used from the program library were Zn = 5.680, F = 5.654, P = 5.13, O = 5.805, and D = 6.674 fm. Observed, calculated, and difference plots of the neutron diffraction powder pattern of $Zn_2(OD)_{0.14(3)}F_{0.86(3)}(PO_4)$ are shown in Fig. 4. The neutron diffraction investigation does not unambiguously prove a partial substitution of OD^- for F^-. The Zn–O/F and P–O bond lengths from this

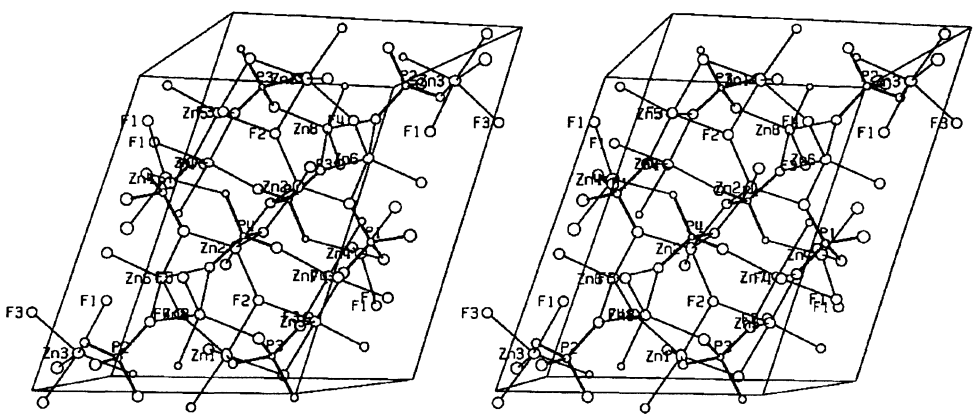

FIG. 3. Projection of the structure for $Zn_2F(PO_4)$ a few degrees off the [010] direction showing half the content of the unit cell.

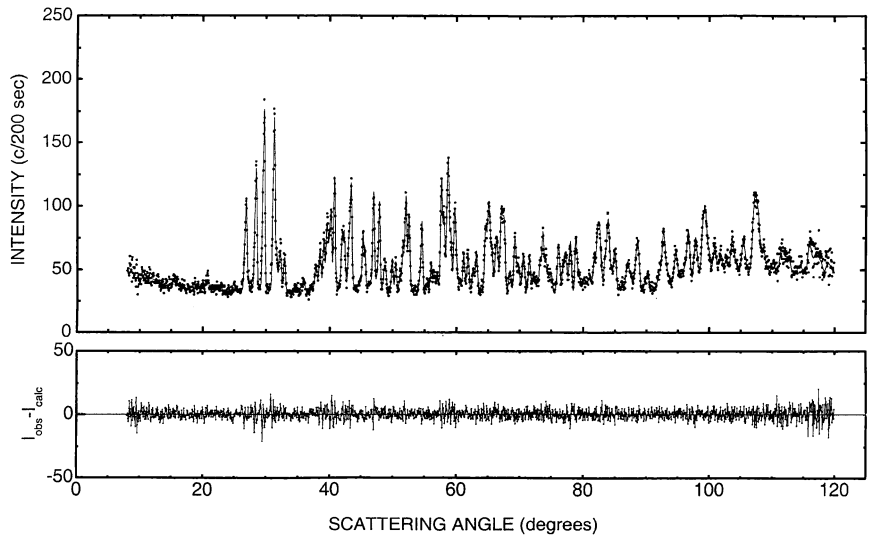

FIG. 4. Profile plot of the neutron diffraction powder pattern of $Zn_2(OD)_{0.14(3)}F_{0.86(3)}(PO_4)$. The experimental data in the upper plot are illustrated by dots while the line corresponds to the result of a GSAS refinement using the positional parameters in Table 3. The lower part shows a difference plot between the experimental and calculated intensities.

calculation did not show any significant discrepancies from the values obtained in the single-crystal X-ray diffraction investigation.

NMR Spectroscopy

The ^{31}P MAS NMR spectrum, obtained with ^{1}H high-power decoupling, of the $Zn_2F(PO_4)$ sample prepared in the H_2O medium is illustrated in Fig. 5a and shows three ^{31}P resonances with relative intensities of 1:1:2, corresponding to four P atoms in the asymmetric unit. The resonance of highest intensity exhibits a shoulder on its high-frequency side. This indicates that the two P atoms, which account for this resonance, have slightly different chemical shifts. A computer deconvolution of the spectrum gives the following isotropic chemical shifts for the four P atoms: $\delta_{iso} = 6.9(1)$ ppm, 5.4(1) ppm, 3.4(3) ppm, and 2.8(2) ppm. These δ_{iso} values and the absence of significant chemical shift anisotropies for the four P sites are in good agreement with chemical shift data reported for orthophosphates (29, 30). The ^{31}P MAS NMR spectrum for the sample prepared in the D_2O medium (not shown) is very similar to the spectrum in Fig. 5, demonstrating that these two samples have identical structures and that none of them contains any P impurities. Furthermore, a ^{31}P–$\{^{19}F\}$ cross-polarization (CP)/MAS NMR spectrum recorded with high-power ^{19}F decoupling shows a minor improvement in resolution of the ^{31}P resonances, in particular at slow-speed spinning, which indicates that the ^{31}P–^{19}F dipolar couplings are not completely removed by slow-speed MAS. The sample from the H_2O synthesis has also been investigated by ^{31}P–$\{^{1}H\}$ CP/MAS NMR resulting in the spectrum shown in Fig. 5b. In this experiment magnetization is transferred from ^{1}H to ^{31}P via ^{1}H–^{31}P dipolar couplings (31) and thereby the experiment detects only ^{31}P sites in close proximity to ^{1}H atoms. Thus, the observation of a ^{31}P–$\{^{1}H\}$ CP/MAS NMR spectrum (Fig. 5b) very similar to the standard ^{31}P MAS spectrum (Fig. 5a) unambigously demonstrates the presence of ^{1}H in the crystallites of $Zn_2F(PO_4)$ either in the form of OH or H_2O. This fact is further supported by the ^{1}H MAS NMR spectrum (Fig. 6) which shows a single resonance at $\delta_{iso} = 2.6(1)$ ppm with a line width of 0.6 ppm. The narrow line width observed without significant spinning sidebands shows that the ^{1}H resonance is not affected by ^{1}H–^{1}H dipolar interactions and thus, that it originates from OH groups and not H_2O in the crystal lattice. A quantitative analysis of the ^{1}H MAS NMR spectrum in Fig. 6, which employs a relaxation delay corresponding to full ^{1}H spin-lattice relaxation, gives the composition of the sample $Zn_2(OH)_xF_{1-x}(PO_4)$, $x = 0.14(3)$, i.e., $Zn_2(OH)_{0.14(3)}F_{0.86(3)}(PO_4)$. The sample prepared in the D_2O medium has been characterized by ^{1}H as well as ^{2}H MAS NMR. The ^{1}H MAS NMR spectrum shows that the sample contains only minor traces of ^{1}H. The ^{2}H MAS NMR spectrum (Fig. 7a) illustrates the manifold of spinning sidebands originating from the $m = 1 \leftrightarrow m = 0$ and $m = 0 \leftrightarrow m = -1$ transitions, which are strongly influenced by the ^{2}H quadrupole coupling interaction. Least-squares fitting of simulated to experimental spinning sideband intensities (17, 18) for the spectrum in Fig. 7a gives the ^{2}H quadrupole coupling parameters $C_Q = 254 \pm 2$ kHz and $\eta_Q = 0.08 \pm 0.02$ for a single ^{2}H site and the optimized simulated spectrum shown in Fig. 7b. The magnitude of the ^{2}H quadrupole coupling constant is in full agreement with

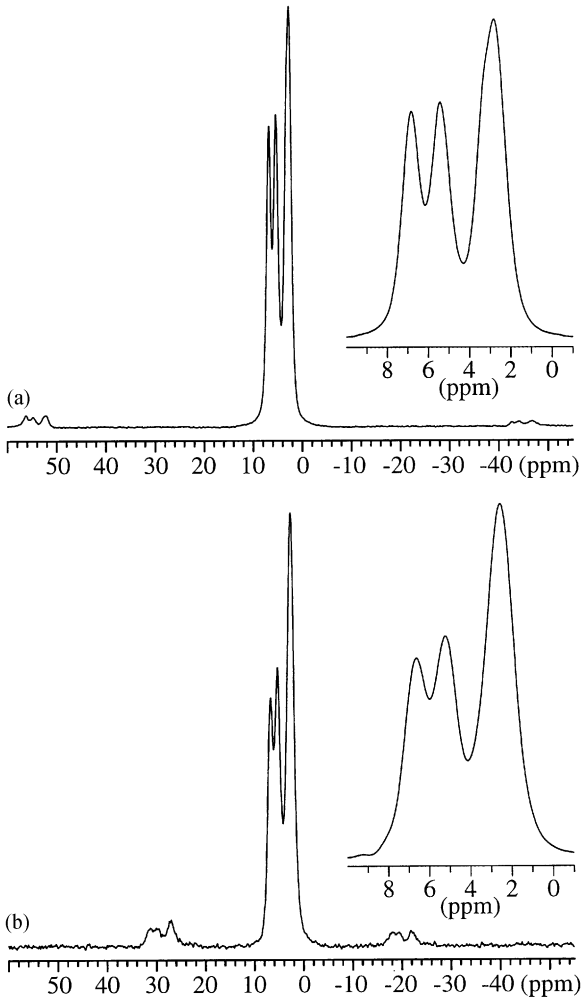

FIG. 5. ^{31}P MAS (a) and CP/MAS (b) NMR spectra of the $Zn_2(OH)_{0.14(3)}F_{0.86(3)}(PO_4)$ sample prepared in a H_2O medium illustrating the observation of three resonances with approximate relative intensities of 1:1:2. The MAS NMR spectrum (a) employed the spinning speed $\nu_R = 8.0$ kHz, a 60-s relaxation delay, and 28 scans, while the CP/MAS NMR spectrum was recorded using $\nu_R = 4.0$ kHz, a CP contact time of 500 μs, a 30-s relaxation delay, and 128 scans.

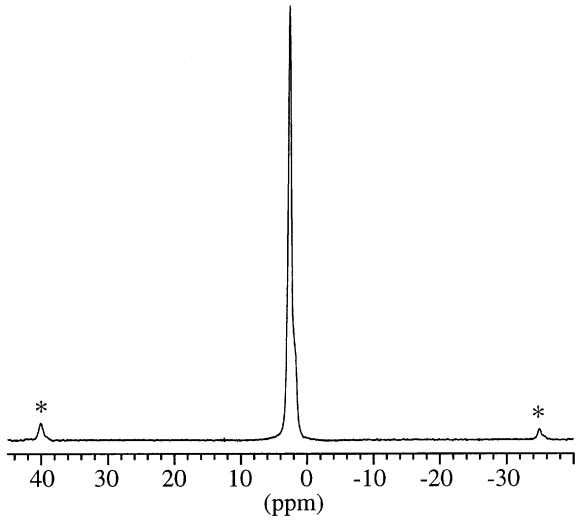

FIG. 6. ^1H MAS NMR spectrum of the $Zn_2(OH)_{0.14(3)}F_{0.86(3)}(PO_4)$ sample prepared in a H_2O medium showing a single resonance at $\delta_{iso} = 2.6$ ppm with a small line width of 0.6 ppm. The spectrum was recorded using the spinning speed $\nu_R = 15.0$ kHz, a 30-s relaxation delay, and 99 scans. The asterisks indicate spinning sidebands.

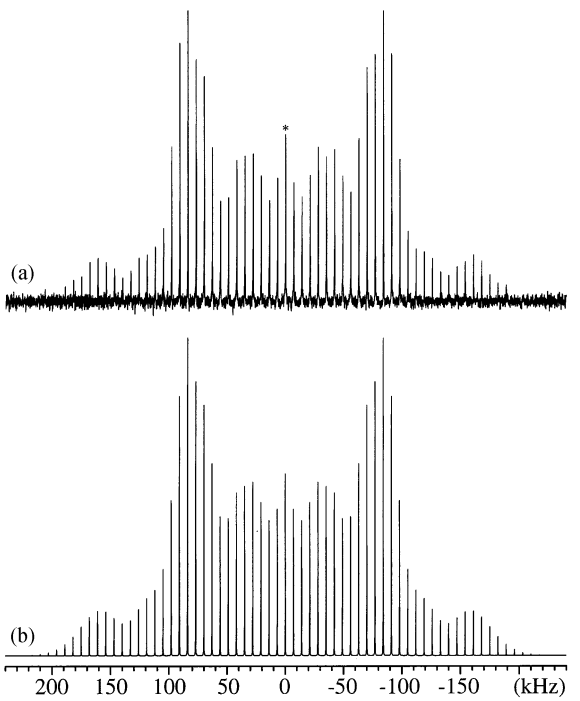

FIG. 7. (a) ^2H MAS NMR spectrum (9.4 T) of the $Zn_2(OD)_{0.14(3)}F_{0.86(3)}(PO_4)$ sample prepared in D_2O recorded with the spinning speed $\nu_R = 7.0$ kHz, a 10-s repetition delay, and 15.400 scans. The spectrum is referenced to the isotropic peak, which is indicated by an asterisk. (b) Simulated spectrum of the manifold of spinning sidebands in (a) corresponding to the optimized ^2H quadrupole coupling parameters ($C_Q = 254 \pm 2$ kHz and $\eta_Q = 0.08 \pm 0.02$).

the presence of OD groups in the sample, since $C_Q(^2H)$ values in the range 245–310 kHz have been observed earlier for inorganic hydroxides (32–34). In contrast, ^2H quadrupole couplings for water molecules in inorganic hydrates are somewhat smaller (i.e., approximately in the range 110–210 kHz at room temperature (34–36)) which may reflect motional averaging of the quadrupole coupling interaction, for example by fast reorientation about the bisecting axis of the water molecule. Thus, the ^2H MAS NMR spectrum strongly indicates that ^2H in the sample is present only as OD groups in agreement with the results from ^1H MAS NMR. Finally, the ^{19}F MAS NMR spectrum (7.1 T, $\nu_R = 11.2$ kHz) of the sample prepared in the D_2O medium (not shown) exhibits two resolved resonances with the

isotropic chemical shifts −176.1(3) and −177.6(3) ppm and almost identical intensity. These resonances are assigned to overlapping resonances from the four distinct fluorine sites in $Zn_2F(PO_4)$. The ^{19}F isotropic chemical shifts are very similar to those observed for ^{19}F in zeolites and layered silicates (37).

CONCLUSION

Single-crystal X-ray diffraction and neutron powder diffaction have been successfully employed in combination with multinuclear solid-state NMR in the characterization and structural analysis of samples of the zinc fluoro phosphate $Zn_2F(PO_4)$ where fluorine ions are replaced by OH^- groups to a small extent. $Zn_2F(PO_4)$ has been prepared by hydrothermal synthesis using hydrofluoric acid as a mineralizer and the crystal structure have been solved from single-crystal X-ray diffaction data. The neutron powder diffraction investigation could not prove the OD^-/F^- substitution in the sample because the neutron scattering contributions from F and O atoms are rather similar and the OD/F substitution is low. However, the ^1H, ^2H MAS and $^{31}P-\{^1H\}$ CP/MAS NMR investigations unambiguously demonstrate the presence of OH groups in the actual structure of $Zn_2F(PO_4)$. A quantitative evaluation of the ^1H MAS NMR spectrum gave the following composition $Zn_2(OH)_{0.14(3)}F_{0.86(3)}(PO_4)$ for the investigated sample.

ACKNOWLEDGMENTS

The Danish Natural Science Research Council has supported this investigation with grants. Carlsbergfondet is acknowledged for the DTA–TGA instrument. Risø National Laboratory is acknowledged for the use of the neutron powder diffractometer. The work at Brookhaven National Laboratory was supported under contract DE-AAC02-98CH10086 with the U.S. Department of Energy, Office of Basic Energy Sciences, Divisions of Chemical Sciences and Material Sciences. The use of the facilities at the Instrument Centre for Solid-State NMR Spectroscopy, University of Aarhus, is acknowledged. Mrs. C. Secher, Mrs. M.-A. Chevallier, and Mr. N. J. Hansen are thanked for valuable assistance. J.S. thanks the Danish Natural Science Research Council for financial support (J. No. 0001237).

REFERENCES

1. S. T. Wilson, B. M. Lok, and E. M. Flanigen, U.S. Patent 4310440, 1982.
2. E. M. Flanigen, B. M. Lok, R. L. Patton, and S. T. Wilson, *Stud. Surf. Sci. Catal.* **28,** 103 (1986).
3. A. Kupermann, S. Nadimi, S. Oliver, G. A. Ozin, J. M. Garcés, and M. M. Olken, *Nature* (*London*) **365,** 239 (1993).
4. A. N. Christensen and R. G. Hazell, *Acta Chem. Scand.* **53,** 403 (1999).
5. "Solid-State NMR Spectroscopy of Inorganic Materials" (J. J. Fitzgerald, Ed.), *ACS Symp. Ser.* Vol. 717. Am. Chem. Soc., Washington, D.C., 1999.
6. G. Cocco, L. Fanfani, and P. F. Zanazzi, *Z. Kristallogr.* **123,** 321 (1966).
7. A. Cordsen, *Can. Mineral.* **14,** 143 (1976).
8. A. Coda, G. Giuseppetti, and C. Tadini. *Atti Accad. naz. Lincei* (*Rc. Cl. Sci. fis. mat. nat.*) **43,** 212 (1967).
9. P. V. Pavlov and N. V. Belov, *Kristallografiya* **4,** 324 (1959).
10. J. R. Rea and E. Kostiner, *Acta Crystallogr. B* **28,** 2525 (1972).
11. M. Leblanc, I. Collin-Fèvre, and G. Férey, *J. Magn. Magn. Mater.* **167,** 71 (1997).
12. J. R. Rea and E. Kostiner, *Acta Crystallogr. B* **30,** 2901 (1974).
13. J. R. Rea and E. Kostiner, *Acta Crystallogr. B* **32,** 1944 (1976).
14. G. Raade and C. Rømming, *Z. Kristallogr.* **177,** 15 (1986).
15. W. T. A. Harrison, J. T. Vaughey, L. L. Dussack, A. J. Jacobson, T. E. Martin, and G. D. Stucky, *J. Solid State Chem.* **114,** 151 (1995).
16. F. C. Hawthorne, *Can. Mineral.* **14,** 143 (1976).
17. J. H. Kristensen, H. Bildsøe, H. J. Jakobsen, and N. C. Nielsen, *J. Magn. Reson.* **92,** 443 (1991).
18. J. Skibsted, N. C. Nielsen, H. Bildsøe, and H. J. Jakobsen, *J. Magn. Reson.* **95,** 88 (1991).
19. G. S. Zhu, F. S. Xiao, S. L. Qui, P. C. Hun, R. R. Xu, S. J. Ma, and O. Terasaki, *Microporous Mater.* **11,** 269 (1977).
20. B. M. Lok, C. A. Messina, P. L. Patton, R. T. Gajek, T. R. Cannan, and E. M. Flanigen, *J. Am. Chem. Soc.* **106,** 6092 (1984).
21. G. S. Pawley, *J. Appl. Crystallogr.* **14,** 357–361 (1981).
22. A. Boultif and D. Loüer, *J. Appl. Crystallogr.* **24,** 987–993 (1991).
23. A. Altomare, G. Cascarano, C. Giacovazzo, A. Gugliardi, A. Burla, M. C. Polidori, and M. Camalli, *J. Appl. Crystallogr.* **27,** 435 (1994).
24. W. R. Busing, K. O. Martin, and H. A. Levy, ORFLS, A Fortran Crystallographic Least Squares Program, Report ORNL-TM 306. Oak Ridge National Laboratory, Oak Ridge, TN, 1962. LINUS is a 1971 version of ORFLS.
25. W. T. A. Harrison, T. E. Martin, T. E. Gier, and G. D. Stucky, *J. Mater. Chem.* **2,** 175 (1992).
26. W. T. A. Harrison, T. M. Nenoff, M. M. Eddy, T. E. Martin, and G. D. Stucky, *J. Mater. Chem.* **2,** 1127 (1992).
27. K. Yvon, W. Jeitschko, and E. Parthé, *J. Appl. Crystallogr.* **10,** 73 (1977).
28. A. C. Larson and R. B. von Dreele, GSAS, General Structure Analysis System, LANSCE, MS-H805, Los Alamos National Laboratory, Los Alamos, NM, 1994.
29. G. L. Turner, K. A. Smith, R. J. Kirkpatrick, and E. Oldfield, *J. Magn. Reson.* **70,** 408 (1986).
30. P. Hartmann, J. Vogel, and B. Schnabel, *J. Magn. Reson. Ser. A* **111,** 110 (1994).
31. A. Pines, M. G. Gibby, and J. S. Waugh, *J. Chem. Phys.* **59,** 569 (1973).
32. T. Chiba, *J. Chem. Phys.* **47,** 1592 (1967).
33. J. O. Clifford, J. A. S. Smith, and F. P. Temme, *J. Chem. Soc., Faraday Trans. 2* **71,** 1352 (1975).
34. E. F. Rakiewics, A. J. Benesi, M. W. Grutzeck, and S. Kwan, *J. Am. Chem. Soc.* **120,** 6415 (1998).
35. J. W. McGrath and G. W. Ossman, *J. Chem. Phys.* **46,** 1824 (1967).
36. G. Soda and T. Chiba, J. Chem. Phys. **50,** 439 (1969).
37. J. M. Miller, *Prog. Nucl. Magn. Reson. Spectrosc.* **28,** 255 (1996).